

endings, along with observed increases in spine density and the appearance of newly formed dendritic branches, suggests that neurons are responding to abnormal cues from the internal or external milieu of the cell. A metabolic disturbance in the neuron, perhaps under the control of the HD gene, may lead to dendritic hyperplasia. Such a condition is thought to account for the appearance of "meganeurites" in cortical pyramidal cells in variants of Tay-Sachs disease in which there is an abnormal accumulation of gangliosides (7). Alternatively, neurons in HD may be influenced by trophic factors in the local environment because of the loss of intrastriatal or extrinsic afferent inputs. Studies in rats have shown that reorientation and growth of dendrites and spines can occur after denervation of the dentate gyrus (20).

The loss of spines in HD is a more variable feature than the recurving of dendrites and may be secondary to other pathological events in the brain. Spine loss in the neostriatum in HD may be dependent on the degree of atrophy or cell loss in the cerebral cortex (2). Cortical neurons provide a major source of afferents to the neostriatum, where they synapse primarily with dendritic spines (21), and experiments have shown that the density of spines in neostriatal neurons is markedly reduced after cortical deafferentation (22). Moreover, a marked loss of spines in neostriatal spiny neurons was observed in one of our diseased controls in which there was extensive damage to the cortex.

In summary, Golgi impregnations of the neostriatum provide morphological evidence that a specific type of neostriatal neuron, the spiny cell, may be selectively altered in HD. Our findings suggest that the dendrites of spiny neurons exhibit a variety of changes in HD which have regenerative and degenerative characteristics. The relative frequency of affected neurons and the types of changes observed can be correlated with their location in the neostriatum.

G. A. GRAVELAND
R. S. WILLIAMS
M. DiFIGLIA*

Department of Neurology,
Massachusetts General Hospital and
Harvard Medical School, Boston 02114

References and Notes

1. G. W. Paulson, *Adv. Neurol.* **23**, 177 (1979).
2. G. W. Bruyn, G. T. A. M. Bots, R. Dom, *ibid.*, p. 83.
3. R. Dom, F. Baro, J. M. Bruchner, in *Huntington's Chorea: 1872-1972*, A. Barbeau, T. N. Chase, G. W. Paulson, Eds. (Raven, New York, 1973), p. 369; H. Lange, G. Thorner, A. Hopf, K. F. Schroeder, *J. Neurol. Sci.* **28**, 401 (1976).
4. H. Braak and E. Braak, *Cell Tissue Res.* **227**, 319 (1982); H. T. Chang, C. Y. Wilson, S. T. Kitai, *J. Comp. Neurol.* **298**, 197 (1982) M.

- DiFiglia, P. Pasik, T. Pasik, *Brain Res.* **114**, 245 (1976); M. Eder, T. Vizkelety, T. Tombol, *Acta Morphol. Acad. Sci. Hung.* **28**, 337 (1980); C. A. Fox, A. N. Andrade, D. E. Hillman, R. C. Schwyn, *J. Hirnforsch.* **13**, 181 (1971/1972); G. A. Graveland, R. S. Williams, M. DiFiglia, *J. Comp. Neurol.*, in press; J. M. Kemp and T. P. S. Powell, *Philos. Trans. R. Soc. London Ser. B* **262**, 383 (1971).
5. M. DiFiglia, P. Pasik, T. Pasik, *J. Neurocytol.* **9**, 471 (1980); M. DiFiglia, N. Aronin, J. B. Martin, *J. Neurosci.* **2**, 303 (1982); R. J. Preston, G. A. Bishop, S. T. Kitai, *Brain Res.* **183**, 253 (1980); P. Somogyi, J. P. Bolam, A. D. Smith, *J. Comp. Neurol.* **195**, 567 (1981); C. J. Wilson and P. M. Groves, *ibid.* **194**, 599 (1980).
6. P. R. Huttenlocher, *Neurology* **24**, 203 (1974); R. S. Williams, S. L. Hauser, D. P. Purpura, G. R. DeLong, C. H. Swisher, *Arch. Neurol.* **37**, 749 (1980).
7. D. P. Purpura, in *Congenital and Acquired Cognitive Disorders*, R. Katzman, Ed. (Raven, New York, 1979), p. 43.
8. A. Scheibel, *ibid.*, p. 107.
9. Wilson's disease is a metabolic storage disease in which the globus pallidus and putamen are atrophic; Parkinson's disease involves a disturbance in the nigrostriatal dopaminergic pathway.
10. Impregnation artifacts due to long postmortem delays, as previously described in rats [R. S. Williams, R. J. Ferrante, V. S. Caviness, Jr., *J. Neuropathol. Exp. Neurol.* **37**, 13 (1978)], were not present in any of the tissues examined in this study.
11. Blocks were placed in an osmium dichromate solution for 2 to 5 days, transferred to 0.75 percent silver nitrate for another 2 to 3 days, and embedded in celloidin. Sections (100 μ m) were cut and mounted in serial order.
12. In normal brains spiny neurons exhibit up to a 5th-order branching, which occurs in the proximal half of the dendritic field. Proximal dendrites are typically spine-free, whereas distal branches are covered with numerous spines.
13. Six of the ten HD group samples were selected for quantitative study because they contained sufficient numbers of impregnated neurons in the caudate and putamen. Slides from the HD and control groups were coded, randomized, and examined under the light microscope at $\times 400$. Sections were scanned systematically and neurons coming into the field of view were evaluated. For each cell, all dendrites that could be followed to their termination were recorded. A bend in the dendrite of 90° or more was established a priori as the criterion for a recurved ending. Results were expressed as the percentage of neurons with recurved dendrites (Fig. 4a) and the percentage of dendrite endings with recurved tips (Fig. 4b).
14. Dendrites (defined here as a stem segment and all its subordinate branches) from the HD and normal control groups were examined for overall length with a computer-assisted light microscope. Dendrites selected for measurement (60 HD group and 29 control dendrites) were optimally oriented in the plane of tissue section. A

calibrated eyepiece reticle and a $\times 100$ oil immersion lens were used. Starting at the dendrite origin, reference points marking 10- μ m segments were entered into the computer [R. S. Williams and S. Matthysse, *J. Comp. Neurol.* **215**, 154 (1983)] and the overall length of the dendrite was determined by adding the segments.

15. Neurons studied for recurved endings (13) were also examined qualitatively for spine density. A neuron was rated as "low" if the density of spines in most dendrites appeared to be less than half that typical of most spiny neurons in normal controls or "high" if spine density in one or more dendrites exceeded that typical of normals. To check the validity of the ratings, spines were counted in some dendrites from cell body origin to termination with a calibrated eyepiece reticle and a $\times 100$ oil immersion lens. The density of spines in normal controls ($n = 10$ dendrites) ranged from six to eight spines per 10 μ m of dendrite. In HD spiny neurons, spine density ranged from three to four spines per 10 μ m ($n = 10$ dendrites) for neurons with a low spine density rating and 12 to 15 spines per 10 μ m ($n = 10$ dendrites) for neurons with a high density rating.
16. It should be emphasized that individual HD neurons could exhibit both atrophic and regenerative changes. For example, a neuron with marked spine loss might also have abnormally long recurved dendrites or dendritic appendages.
17. J. P. Bolam, P. Somogyi, H. Takagi, I. Fodor, A. D. Smith, *J. Neurocytol.* **12**, 325 (1983); M. DiFiglia, N. Aronin, J. B. Martin, *J. Neurosci.* **2**, 303 (1982); C. E. Ribak, J. E. Vaughn, E. Roberts, *J. Comp. Neurol.* **187**, 261 (1979).
18. P. C. Emson, A. Arregui, V. Clement-Jones, B. E. B. Sandberg, M. Rossor, *Brain Res.* **199**, 147 (1980); T. L. Perry, S. Hansen, M. Kloster, *N. Engl. J. Med.* **288**, 337 (1973).
19. On the basis of our clinical records, this is unlikely to be a pharmacological effect. Of the six HD patients studied quantitatively, two were on haloperidol, one was on Benadryl, and two were not taking any medication. No information on the other patient was available. One of the two psychotic patients (77 years old) was on phenothiazines.
20. J. G. Parnavelas, G. Lynch, N. Brecha, W. W. Cotman, A. Globus, *Nature (London)* **248**, 71 (1974); A. Cacereo and O. Steward, *J. Comp. Neurol.* **214**, 387 (1983).
21. R. Hassler, J. W. Chung, U. Rinne, A. Wagner, *Exp. Brain Res.* **31**, 67 (1978); J. M. Kemp and T. P. S. Powell, *Philos. Trans. R. Soc. Ser. B* **262**, 413 (1971).
22. J. M. Kemp and T. P. S. Powell, *Philos. Trans. R. Soc. Ser. B* **262**, 429 (1971).
23. Supported by NIH grants NS 16367 (M.D.), MH34079 (R.S.W.), and MH-NS31862 (E. Bird). We are grateful to E. Bird for help in obtaining tissue and to N. Aronin and R. Brown for helpful suggestions on the manuscript.

* To whom correspondence should be addressed.

20 August 1984; accepted 16 October 1984

Computer Graphics Representation of Levels of Organization in Tobacco Mosaic Virus Structure

Abstract. *Methods for simplifying computer graphics images of atomic models of complex macromolecular assemblies have been applied to the tobacco mosaic virus structure to display different levels of its organization. By constructing sharply outlined pictures of the parts of the virus particle with the image resolution reduced or with obscuring detail eliminated, aspects of the subunit packing and chain folding are distinctly illustrated.*

Structures of increasingly complex macromolecular assemblies are being solved to the atomic level by x-ray diffraction analysis. Computer graphics methods have been applied to macromolecular structures to produce high-resolution color pictures of the molecular surfaces (1) and to display details of

surface interactions and the underlying skeletal structure (2). Regardless of whether the atomic arrangements are represented by space-filling or by skeletal models, only relatively small portions of complex molecules can be effectively visualized at one time. The foldings of protein backbones into α -helical and β -

sheet conformations have been illustrated by schematic ribbon drawings (3), and stereo-pair schematic diagrams have been generated by computer graphics (4). Proceeding to higher levels of macromolecular organization requires the construction of even simpler images to represent subunit packing arrangements.

We have developed computer graphics methods for simplifying images of molecular models of complex structures to focus on different levels of organization. Starting with an atomic model of the tobacco mosaic virus (TMV) coat protein and the RNA in the helical virus particle (5), we show how the information contained in the molecular model can be reduced to display the chain folding and subunit packing. Application of these procedures to images of TMV will facilitate the correlation of the information on the virus particle assembly and stability (6, 7) with its molecular structure, which has been determined at 3.6-Å resolution (5). Furthermore, these methods should be generally applicable to other macromolecular assemblies for illustrating the ways in which complex biological structures are built.

The simplest type of picture is a black-and-white outline. Line drawings, which may contain only minimal information, can convey profound impressions, as is evident in the work of master artists. Adding depth-cueing and shading to the outline can assist in perception of three-dimensional shapes, but too much detail may obscure basic forms. Color may be used to code for additional information—for example, to distinguish chemical composition or sequence position—but again excessive information may be confusing. We have sought to generate simple, stereo-pair outline drawings of basic molecular shapes at different levels of resolution that can be selectively embellished by depth cueing, surface shading, and color coding (8).

Construction of the computer graphics drawings starts with a three-dimensional electron-density map calculated from the atomic coordinates of all or any part of the molecular model. Atoms are represented as gaussian spheres of half-width corresponding to the resolution chosen for the display; alternatively, the atoms can be represented as hard spheres. Densities are sampled on a three-dimensional grid, with the z axis taken as the direction of view, and are stored in the core memory of a VAX 11/780 computer. Two-dimensional images are produced by scanning along the z axis and storing the z coordinate of the first sampled density that is greater than a threshold

chosen to represent the molecular surface. The atom type for chemical coding or residue number for sequence coding is also stored for each two-dimensional sampling point. Lines are generated to represent two types of edge: external edge lines (defined by the sampled points that are adjacent in x or y directions to nonsampled points) are drawn thicker than internal edge lines (defined by the sampled points whose z coordinate is two or more grid units greater than that of an adjacent sampled point). Brightness is used to indicate both depth and shape. Brightness used for depth cueing is determined by the z coordinate of the sampled points within the boundary lines. Brightness indicating shape (by simulating the effect of directional illumination) is added to that cueing depth. The shading for shape is determined by the angle between the surface normal vector at each point and a reference vector corresponding to a direction of illumination. No shadows, however, are cast by one part of the structure on another, because this would confuse the image. The total brightness number can be combined with a color code number for chemical composition or sequence position. The final image is displayed in a 512 by 512 picture element array on an AED raster graphics terminal in black and white or in color (9).

The stereo-pair atomic model of the TMV protein subunit viewed from the direction taken to be the top of the virus helix (Fig. 1a) was constructed by representing the atoms as hard spheres 2 Å in diameter; the use of undersized atoms allows some interior portions of the structure to be seen. Atoms are color-coded to distinguish carboxyl oxygens, cationic nitrogens, nonionic side-chain oxygens and nitrogens, aromatic groups, aliphatic side chains, and the peptide backbone. Depth is indicated by shading from light to dark colors. No matter what scheme is used to represent the atomic structure, there is a confusion of detail that obscures the backbone folding and side-chain interactions.

The stereo-pair model of the backbone of the TMV subunit with the same orientation as the whole molecule (Fig. 1b) was constructed with only the α carbon and the peptide nitrogen and carbon atoms represented as gaussian spheres 3 Å in half-width. A density level for the surface contour was selected by trial and error so that the backbone was represented as a smooth filament about 2.5 Å in diameter. The choice of an oversized gaussian sphere for the backbone atoms and a high-density contour level for the

surface produces a tube of uniform density that is easier to follow than vectors connecting α carbons. This image was colored according to sequence position, starting with the amino terminal end in yellow and progressing through orange to red at the carboxyl terminus. The sequence color coding assists the eye in following chain continuity where more than two segments overlap. To accentuate the coiling and bending of the backbone, the intensities of the colors have been graded to indicate depth and surface shape. Equal ranges of brightness were used for the depth cueing and surface illumination. An orthogonal projection of the backbone trace of the subunit, viewed from the right side (Fig. 1c), was constructed with the same display scheme as for Fig. 1b. These two stereo pairs contain sufficient information to reconstruct a three-dimensional model of the backbone.

Contacts between pairs of subunits could be illustrated by adding the interacting side chains to the backbone trace. However, such a representation is too complicated to show clearly the subunit packing in the virus helix. For distinct representation of the structure of assemblies, the amount of information in the subunit image needs to be reduced.

A simple, low-resolution image of the subunit was generated by making the atoms gaussian spheres about 6 Å in diameter and choosing a density level for the surface contour that gives an approximately correct molecular volume (Fig. 1, d and e). The color range from light yellow to dark brown is used only to present information about the depth and slope of the surface. Black and white could also have been used for this display, but the nearly monochrome yellow scale enhances perception of nuances in the shading. An image of the virus particle without excessive detail can be built up from this simplified subunit model.

Methods used in constructing the early drawing of TMV (6) (Fig. 2a) provided a guide in developing the computer graphics procedures used to represent the virus morphology (Fig. 2b). In 1959, when the drawing in Fig. 2a was made, little was known about the subunit structure; an arbitrary, compact, asymmetric shape was devised for the subunit with as little detail as possible and this model was projected with the helical symmetry of the virus particle, conserving only the outline of the hypothetical subunit. In 1984, with the determination of an atomic model of the subunit, the graphics problem was to reduce this detailed information to a simple outline, with some

Fig. 1. Stereo-pair views of the TMV protein subunit structure showing different levels of detail. The overall length of the molecule in these projections is 70 Å. (a) Atomic model (5) viewed from the top of the virus helix (see Fig. 2). The outside end of the subunit (corresponding to a radius of about 90 Å in the virus helix) is at the left of the figure, and the subunit's right side (11) is facing down. The color coding of the atoms is as follows: red, carboxyl oxygens; blue, cationic nitrogens; pink, nonionic oxygens; light blue, amide nitrogens; purple, aromatic groups; brown, aliphatic side chains; and white, peptide backbone. The colors are shaded from light to dark (for example, white to gray) to indicate depth from the top surface. (b and c) Backbone trace viewed from the top (b) and from the right side (c). The amino terminal end is colored yellow, the carboxyl terminal end is red, and the color changes smoothly from one end to the other. Starting from the amino terminus, the chain passes through part of a β sheet, then into the left-slewed and back to the right-slewed α -helical segments (11), then folds under to the right-radial α helix and around in the inner loop to the left-radial α helix and out to the carboxyl terminus. The inner loop segment, which is disordered in the disk aggregate (12), is shown here in its ordered conformation in the virus. (d and e) Surface views from top (d) and right side (e) of low-resolution model. The orientation in (d) is identical to that in (a) and (b), and the orthogonal view in (e) is identical to that in (c). The folding of the chain is not obvious from the low-resolution surface views, but the chain continuity can be identified by comparison with the backbone traces.

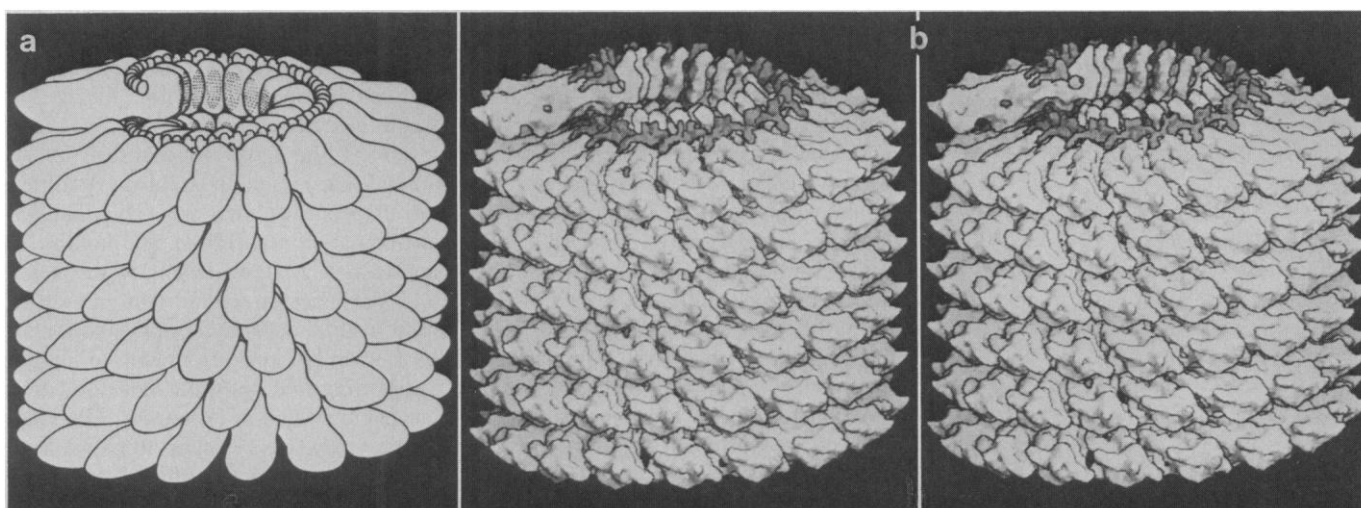
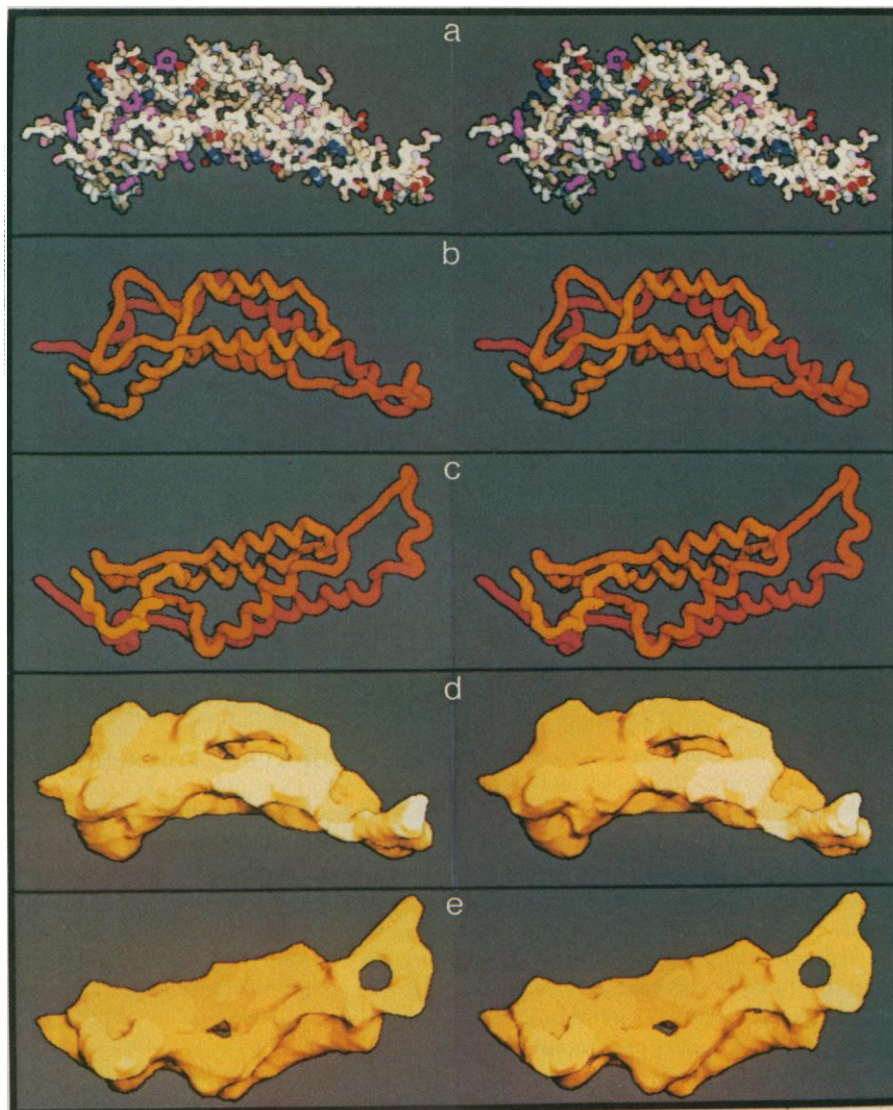


Fig. 2. Old and new images of the TMV helix. The diameter of the particle is 180 Å and the pitch of the helix is 23 Å. (a) Drawing made before the protein structure was known, designed to illustrate the helical packing arrangement (6). (b) Computer graphics, stereo-pair drawing constructed from the low-resolution model of the protein subunit shown in Fig. 1, d and e. The RNA is represented by the dark chain exposed at the top of the virus helix. This simplified image, representing the subunit shape and packing arrangement with the RNA in the virus particle, has been produced by reducing the information from the atomic model.

shading indicative of the underlying molecular substructure. The stereo-pair, black-and-white image of the virus (Fig. 2b) was generated in the computer, taking the same direction of view as in Fig. 2a, by adding together separate projections of the low-resolution subunit model related by the screw symmetry of the virus helix (10). The RNA chain coiling over the top turn of the helix of protein subunits (Fig. 2b) was imaged at about a 4-Å resolution. Bumps on this chain, oriented sequentially (one extending out radially and two extending up), represent the three nucleotides associated with each protein subunit. The interlocked arrangement of the protein subunits and RNA chain (Fig. 2b) can be related to more detailed images of the parts to explain the higher levels of organization in terms of the specific molecular interactions.

We have aimed for a display that keeps the scale of detail in proportion to the overall dimensions of the image: in the distant view, only essential outlines of the parts are conserved; by zooming into the structure, the molecular detail can be augmented as the scale is magnified. This goal could not be realized by constructing an atomic model of the entire virus assembly and then displaying it at low resolution, since this would blur the subunit boundaries. Controlled reduction of image information will facilitate the display and interpretation of the structures of complex macromolecular assemblies.

KEIICHI NAMBA*

DONALD L. D. CASPAR

*Structural Biology Laboratory,
Rosenstiel Basic Medical Sciences
Research Center, Brandeis University,
Waltham, Massachusetts 02254*

GERALD J. STUBBS

*Department of Molecular Biology,
Vanderbilt University,
Nashville, Tennessee 37235*

References and Notes

1. R. J. Feldmann, *Annu. Rev. Biophys. Bioeng.* **5**, 477 (1976); ———, D. H. Bing, B. G. Furie, B. Furie, *Proc. Natl. Acad. Sci. U.S.A.* **75**, 5409 (1978).
2. R. Langridge, T. E. Ferrin, I. D. Kuntz, M. L. Connolly, *Science* **211**, 661 (1981); P. A. Bash, N. Pattabiraman, C. Huang, T. E. Ferrin, R. Langridge, *ibid.* **222**, 1325 (1983).
3. J. S. Richardson, *Adv. Protein Chem.* **34**, 168 (1981).
4. A. M. Lesk and K. D. Hardman, *Science* **216**, 539 (1982).
5. The atomic coordinates were determined by fitting the sequence to a 3.6-Å resolution map of the virus calculated from x-ray fiber diffraction data, phased by multidimensional isomorphous replacement [G. J. Stubbs *et al.*, *Nature (London)* **267**, 216 (1977); K. Namba and G. J. Stubbs, *Acta Crystallogr.*, in press].
6. D. L. D. Caspar, *Adv. Protein Chem.* **18**, 37 (1963).
7. G. J. Stubbs, in *Biological Macromolecules and Assemblies*, F. Journak and A. McPherson, Eds. (Wiley, New York, 1984), p. 149; P. J. G. Butler, *J. Gen. Virol.* **65**, 253 (1984).
8. The graphics programs are written in Fortran and can be used to display structures of any type for which three-dimensional density maps can be calculated (for example, from atomic model coordinates or from x-ray diffraction, electron microscope, or optical data).
9. The Fortran graphics programs use the library subroutines supplied with the AED512 terminal to transfer the image from the core to the raster graphics screen. The programs could easily be adapted for any raster graphics terminal with corresponding subroutines. An integer between 0 and 255 is assigned to each pixel for the screen of the AED512 terminal, and each integer corresponds to a particular brightness and color taken from a table. For example, the color table could include 10 different colors (combinations of red, green, and blue) each with 25 levels of brightness, or 16 colors with 16 levels of brightness, and so on. For black and white images, 256 levels of brightness are available.
10. A two-dimensional image of each subunit in a six-turn helix segment was constructed in the computer. Because there are 49 symmetrically related subunits in the three-turn repeat of the helix, there are 49 different subunit orientations, some of which are hidden in the combined projected image. The individual subunit images, related by the helical symmetry, were combined by comparing z coordinates of corresponding pixels in the overlapping images to remove all hidden parts (that is, at each sampled point only the image pixel with the smallest z coordinate was displayed). The subunit boundaries are marked clearly in the virus image since it is built by adding together the images of the separate, and sharply outlined, subunits.
11. The definition of directions in the subunit and the terminology for the four major α -helical segments follows the nomenclature adopted to describe the protein structure in the two-turn disk aggregate [J. N. Champness, A. C. Bloomer, G. Bricogne, P. J. G. Butler, A. Klug, *Nature (London)* **259**, 20 (1976)]. The ordered part of the protein in the disk aggregate corresponds to the subunit structure in the virus helix at radii greater than 40 Å.
12. A. C. Bloomer, J. N. Champness, G. Bricogne, R. Staden, A. Klug, *Nature (London)* **276**, 362 (1978).
13. We thank D. Hellerstein for help with the computer graphics programming. Supported by U.S. Public Health Service grants GM 25236 and GM 33265 (G.J.S.) and CA 15468 (D.L.D.C.). The VAX 11/780 computer was provided from Shared Instrument grant GM 21189-09S1 awarded to D. J. DeRosier.

* Present address: Department of Molecular Biology, Vanderbilt University, Nashville, Tennessee 37235.

6 August 1984; accepted 23 October 1984

Two Gustatory Systems: Facial and Vagal Gustatory Nuclei Have Different Brainstem Connections

Abstract. *The gustatory sense in catfish consists of two dissociable components, a facial nerve system used for food selection and a vagal nerve system involved in swallowing. Neural tracing experiments demonstrate that the primary sensory nucleus for the facial gustatory system is connected to the reticular formation and trigeminal nuclei. In contrast, the primary sensory nucleus for the vagal gustatory system is connected to the motoneurons that mediate swallowing. These results provide anatomical evidence for parallel gustatory systems within the vertebrate central nervous system.*

Of all the sensory systems, the gustatory sense occupies a unique position at the portal to the alimentary canal. The sense of taste, however, is not limited to reflexive control of swallowing (1, 2), but plays an important role in food selection and determination of palatability. The location of taste buds within the oral cavity appears related to their function; taste buds located most externally are implicated in food selection and appreciation, while taste buds lying closest to the alimentary canal are concerned with ingestive and protective reflexes (2, 3). This dichotomy of function parallels the pattern of innervation of the different groups of taste buds. Taste buds lying closest to the esophagus—for example, on the palate and larynx—are innervated by branches of the vagus nerve; those lying most externally—for example, on the anterior part of the tongue or across the lips and barbels of certain fishes—are innervated by the facial nerve (4, 5). The glossopharyngeal nerve innervates taste buds lying between these extremes.

In catfish, the distinction between the facial and vagal gustatory systems is especially clear. Each nerve terminates

in a separate lobe protruding from the dorsal surface of the rostral medulla. Electrophysiological experiments show that the facial and vagal gustatory lobes receive similar chemosensory input from their respective gustatory fields (6). Nonetheless, selective lesion experiments demonstrate a behavioral dissociation of function for the facial and vagal gustatory lobes (2). A bilateral lesion of the facial lobe results in an animal that is unable to locate food pellets in the surrounding water but that will swallow food placed in its mouth. In contrast, a bilateral lesion of the vagal lobe produces an animal that can locate food in its environment and take it into its mouth, but appears unable to initiate swallowing and spits out any food that has accumulated in its mouth. The glossopharyngeal nerve seems to play a lesser role in gustatory-mediated behaviors in catfish. We have attempted to delineate the anatomical bases for the differences in behavior mediated by the facial and vagal gustatory subsystems.

Horseradish peroxidase (HRP) was used as an anterograde and retrograde tracer of neuronal connectivity in bull-